Supporting Information for Switchable Plasmonic-Dielectric Resonators with Metal-Insulator Transitions

Nikita A. Butakov[1], Ilya Valmianski[2], Tomer Lewi[1], Christian Urban[2], Zhensong Ren[3], Alexander A. Mikhailovsky[4], Stephen D. Wilson[5], Ivan K. Schuller[2], Jon A. Schuller[1]
[1]*University of California, Santa Barbara, Department of Electrical & Computer Engineering*
[2]*University of California, San Diego, Department of Physics and Center for Advanced Nanoscience*
[3] *Boston College, Physics Department*
[4]*University of California, Santa Barbara, Department of Chemistry and Biochemistry*
[5]*University of California, Santa Barbara, Materials Department*
e-mail address: schuller@ece.ucsb.edu

Methods

Growth and Fabrication

Single crystals of VO_2 have been grown by the isothermal flux-evaporation method[1]. The crystal growth was taken place under well controlled gas environment in a Vertical Molysili Furnace from Crystal Systems Corp. The starting material V_2O_5 in powder form was loaded into a platinum crucible and hanged at the heating zone center of the furnace. A controlled flow of CO_2 was fed into the bottom of the furnace and left out at the top. The furnace temperature was raised to 1220 °C and held for about two days in the flow of CO_2 and finally quenched to room temperature. VO_2 crystals were etched from the boule via a dilute aqueous solution of Na_2CO_3.

The VO_2 films were prepared by reactive magnetron sputtering on (012) oriented Al_2O_3 from an in house produced V_2O_3 target[2]. The target was manufactured by pressing Noah Technologies 99.9% purity V_2O_3 powder followed by a 15 hour sintering process under Ar/H(2%) atmosphere at 1050 ^oC. The sputtering was performed in a high vacuum system (base pressure of 1×10^{-7} Torr) backfilled with 4 mTorr ultrahigh purity (UHP-99.999%) Ar/O(8.5%) gas mixture. The substrate temperature was kept at 600 ^oC. Structural purity of the powder, the target, and the films was confirmed by x-ray diffraction. In many other growth methods, the as-deposited films are oxygen-deficient and require annealing in an oxygen environment. In our approach, the relatively high substrate temperature and reactive sputtering in an oxygen environment results in as-deposited films with the correct stoichiometry. The VO_2 films are morphologically granular but crystallographically textured in both in-plane and out-of-plane directions due to the presence of a several monolayer thick strain-relaxation interfacial layer[3].

VO_2 spheres (SEM shown in Fig. S1a) were fabricated by femtosecond laser ablation. We used a commercial femtosecond laser system (Spitfire, Spectra Physics) delivering 1 mJ pulses, with ~120 fs duration, a central wavelength of 800 nm, and a variable repetition rate. The laser output power was controlled by a series of reflective and neutral density glass attenuators and focused on the substrate with a 1 in. focal length lens. The target wafers were mounted on a motorized translation stage (scanning speed of ~ 2 mm/sec) to produce a series of ablation spots separated by ~200 μm. Each ablation spot was created by a single pulse of beam diameter of 50μm, which generated multiple particles. Pulse energies ranging between 20 and 100 μJ, at a 20 Hz repetition rate, were used in ablation experiments. More details on ablation experiments can be found in a previous work[4].

The wire arrays (Fig. S1b) and disk arrays (Fig. S1cd) were fabricated by pattering thin-films with electron-beam lithography, using ma-N 2403 resist. A SiO_2 hard-mask was then deposited and etched with a CF_4 ICP RIE process. The VO_2 film was etched with an Ar/Cl_2 RIE process with 10 sccm Ar and 30 sccm Cl_2. A variety of arrays, with a range of resonator geometries and pitches was fabricated, each 250 μm x 250 μm in size. Due to film surface roughness, the final disk resonators possess a rounded upper surface, which has the effect of shifting the resonant frequency and reducing the overall magnitude of the reflection.

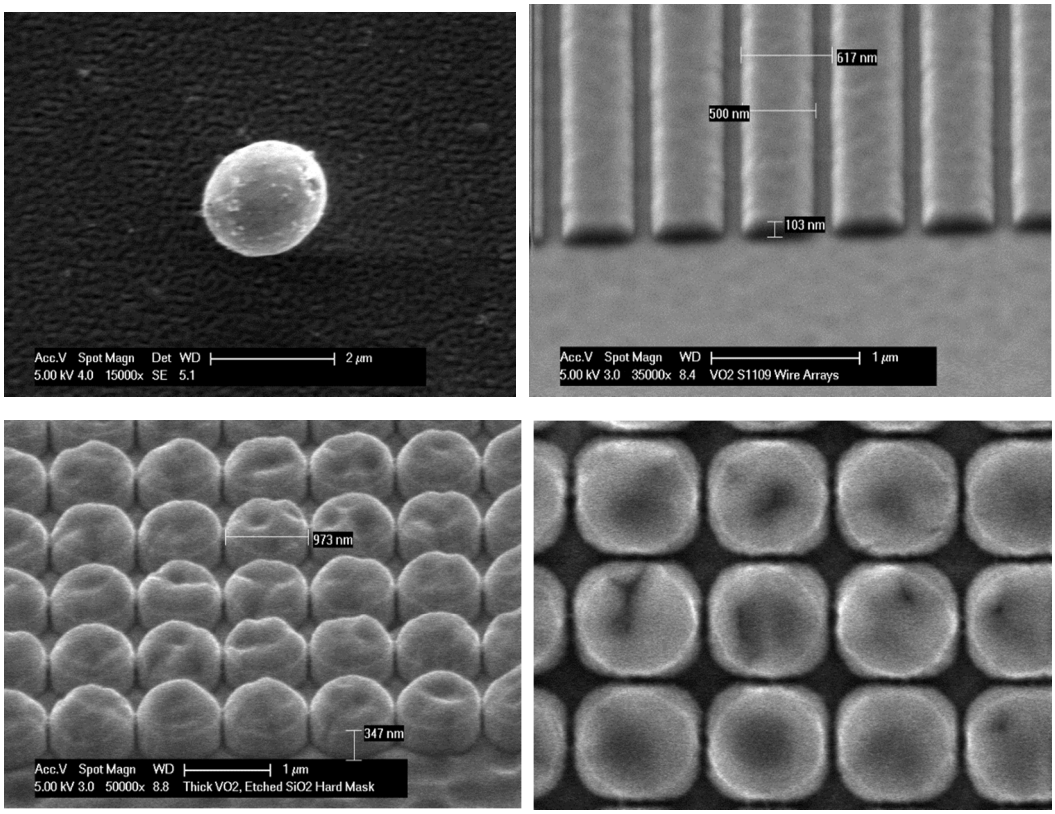

Figure S1 – **Enlarged SEMs of VO2 Structures. (a)** SEM of a VO2 sphere generated by femtosecond laser ablation. **(b)** SEM of a VO2 rod array fabricated by electron-beam-lithography and reactive-ion-etching. **(c,d)** SEMs of a VO2 disk array, at 45 degrees for (c), and normal incidence for (d), fabricated by electron-beam-lithography and reactive-ion-etching.

Optical Characterization

The temperature-dependent reflection and transmission spectra of the VO_2 resonators were measured with a Bruker Vertex FTIR and Hyperion Microscope with a Linkam Heating Stage. For the case of the VO2 single crystals, thin-films, wire arrays, and disk arrays the background spectrum was a 100 nm thick gold film. For the case of the VO2 spheres, the background spectrum was the adjacent area, at the same temperature as the VO2 sphere. Simplified diagrams of the optical path in the reflection and transmission configurations are show in Fig. S2. Resonators were identified and focused using visible light in the microscope. A knife-edge aperture was used to restrict light collection to the area in the vicinity of the resonators. Near-infrared spectra were measured with the InGaAs detector. Mid-infrared spectra were measured with the MCT detector. Optical permittivity models were extracted by fitting a Drude-Lorentz oscillator model to reflection data with RefFIT. The fitted model assumed a Drude free-carrier contribution, a Lorentzian absorption term (which leads to the partial increase of permittivity in Fig. 2b at 339 and 341 K), a semi-infinite sapphire substrate, and that light was normally incident. Although the use of a NA=0.4 lens involved incident light over -23.58 to +23.58 degrees, we found that this was a minor perturbation. The dielectric model did not explicitly include air voids; however, the retrieved optical permittivity can be viewed as an effective response of a VO_2-air mixture. Based off of previous work on V_2O_3[4], we estimate the air void content to be approximately 6%.

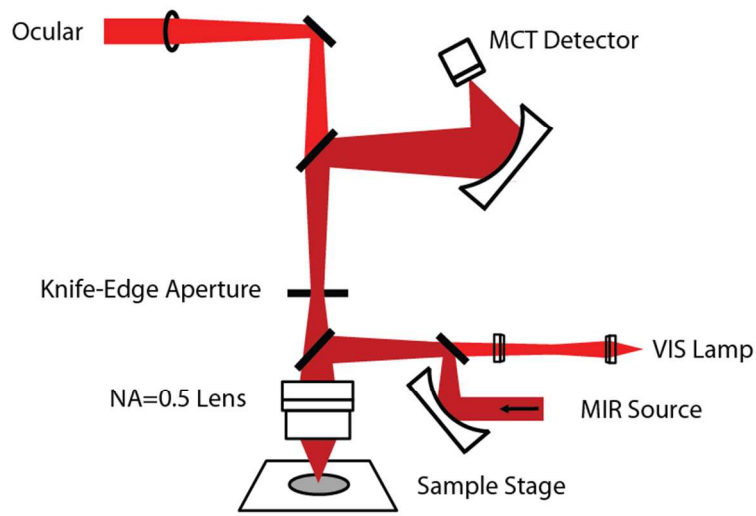

Figure S2 – **Schematic of Optical Setup**

Mie Theory Calculations

The scattering-cross-sections, and the corresponding multipolar contributions, of the VO_2 spheres were calculated using in Mathematica with the Mie Theory formalism[5,6].

Simulations

All electromagnetic simulations were performed with the Lumerical FDTD Solver. Individual disk resonators were simulated with PML boundary conditions and boundaries at least 5 um away from the resonator. The resonator was excited with a total-field-scattered-field source. The total scattering cross section was measured using the built-in 'cross-section' analysis object. Disk resonator arrays were simulated with PML boundary conditions in the z direction, and periodic boundary conditions along the x and y directions, and with an anti-symmetric condition applied along the x-direction and symmetric condition applied along the y-direction to improve computational efficiency. The disks were excited with a plane-wave source. The reflection and transmission scattering parameters were computed with the built-in 's_params' analysis object.

Film Roughness

Film roughness can have substantial effects on the optical response of thin films and resonators. At sufficiently short wavelengths, diffuse scattering due to thin film roughness causes specular reflection and transmission to decrease. In resonators, roughness can lead to an increase in scattering losses and thereby broaden resonances. In this work, the 100 nm film has a relatively small RMS roughness of 5 nm (Fig. S3a), which has a negligible effect on the infrared optical response. The 500 nm film however, has an RMS roughness of 41 nm (Fig. S3b), which causes the measured FTIR reflectivity to drop at short wavelengths, and broadens the resonator optical response.

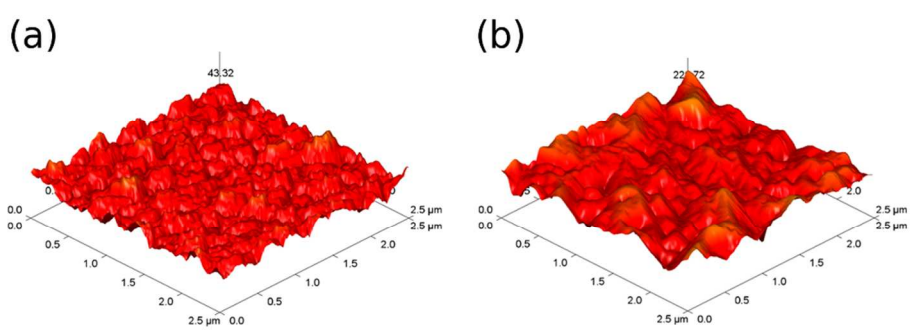

Figure S3 – **Effect of Roughness of VO_2 Thin Films.** The AFM-measured height profile of the **(a)** 100 nm film, and **(b)** 400 nm film. The simulated effect of roughness on the **(c)** 100 nm film, and **(b)** 400 nm film.

Transport Measurements

In Figure S4 we plot the measured sheet resistance of the 100 nm and 400 nm thick VO2 films. In the fully insulating and fully metallic states the thicker film exhibits a lower resistance, consistent with expectations based on optical measurements. Although one would normally expect a thicker film to exhibit larger contrast in sheet resistance and steeper hysteresis, we believe there are differences in the quality of the 100 nm and 400 nm films that are responsible for these differences. We believe the 100 nm film is high-quality, but that the 400 nm film may be mixed-phase with potential gradients in stoichiometry. This may also be responsible for the inability to achieve a strong fit of the optical constants to the 400 nm film.

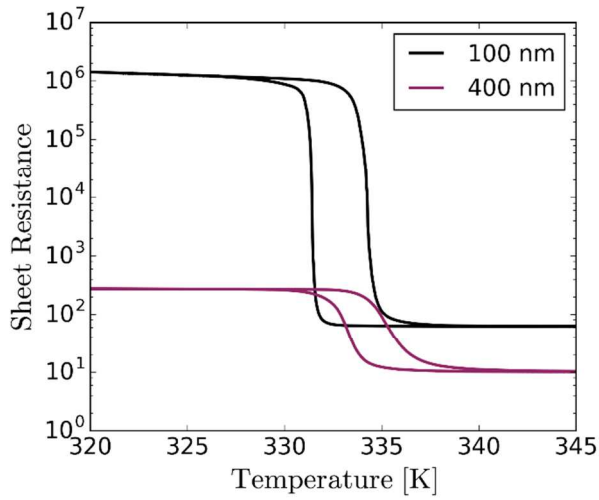

Figure S4 – **Transport Measurements of VO_2 Thin Films**

Single-Crystal Reflectivity over Mid-Infrared Spectrum

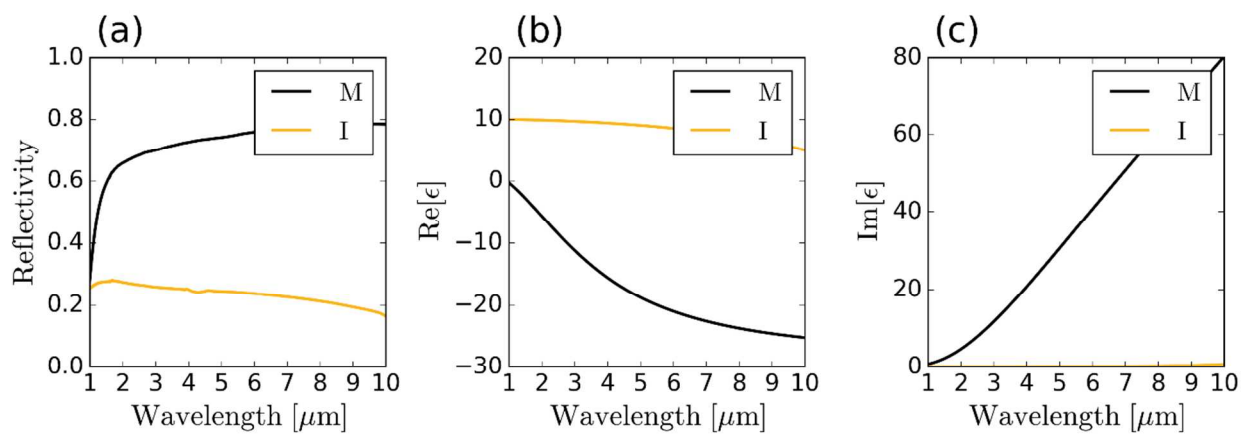

Figure S5 – **VO_2 Single-Crystal Reflectivity. (a)** Reflectivity of a VO_2 single crystal in its insulating (orange) and metallic (black) phases. **(b)** Real, and **(c)** imaginary components of the fitted VO_2 optical permittivity in its insulating (orange) and metallic (black) phases.

Thin-Film Reflectivity over Mid-Infrared Spectrum

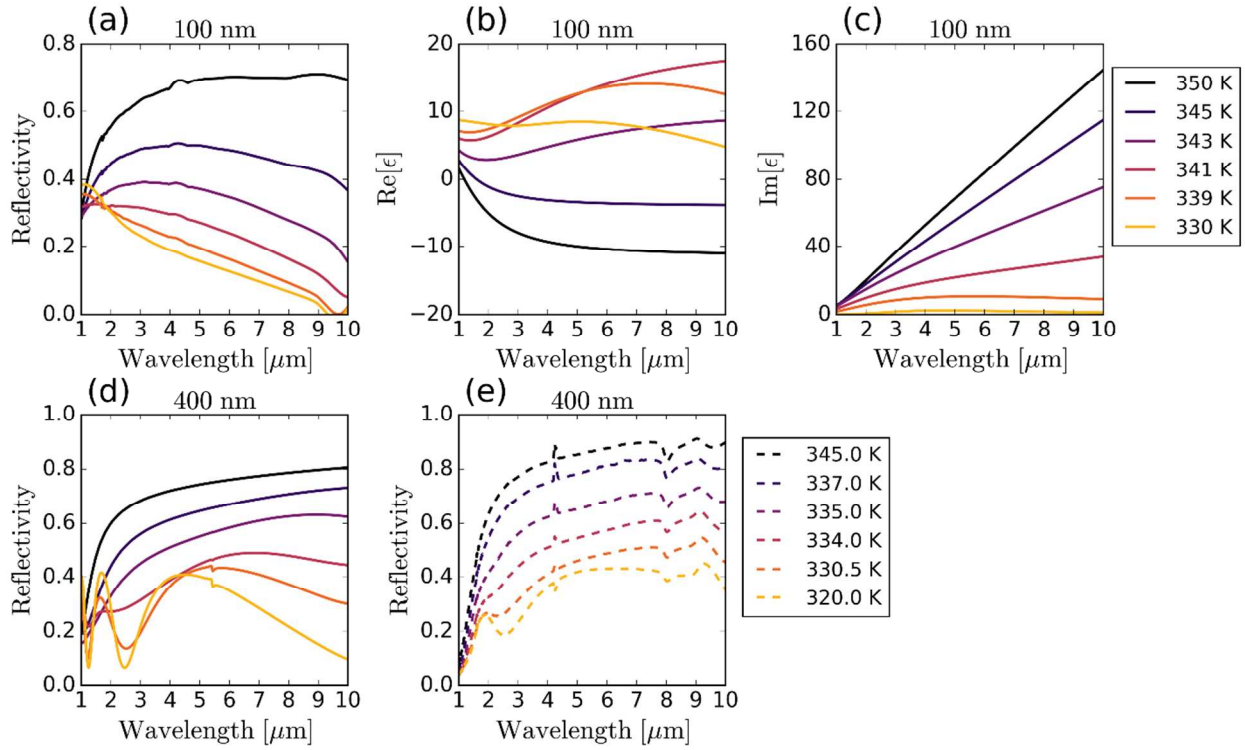

Figure S6 – **VO_2 Thin-Film Reflectivity and Optical Constants (a)** The measured FTIR reflectivity of a 100 nm VO_2 film on a sapphire substrate. The **(b)** real, and **(c)** imaginary components of the optical permittivity, as determined by a spectral fit to the measured reflectivity. (d) A simulation of a 400 nm thick film, based on the 100 nm optical constants. (e) The experimentally measured reflection of a 400 nm thick film.

Random Arrays

We first consider the behavior of randomly positioned clusters of VO_2 nanoparticles, which have an optical response similar to isolated nanoparticles. Using the previously extracted optical constants, in Fig. S7a we plot the simulated extinction-cross-section (ECS) of an individual VO_2 resonator on a sapphire substrate. In the insulating phase (magenta curve), when the permittivity is positive, dielectric Mie resonances are supported. At λ=1.12 μm in particular, there is a sharp peak corresponding to a magnetic quadrupole mode, as can be seen in the internal electric and magnetic fields shown in Fig. S7b. As the VO_2 is heated (Fig. S7c), the real part of the permittivity initially decreases, causing a blue-shift in the resonances, and the imaginary part increases, causing a broadening of the resonances. Around the epsilon-near-zero condition, scattering is suppressed across the spectrum, similar to previously reported behavior in doped semiconductors. Once the VO_2 has been sufficiently heated, the real part of the permittivity becomes negative, and the resonators support a plasmonic electric dipole mode, appearing as a broad resonance peaking at λ=1.37 μm.

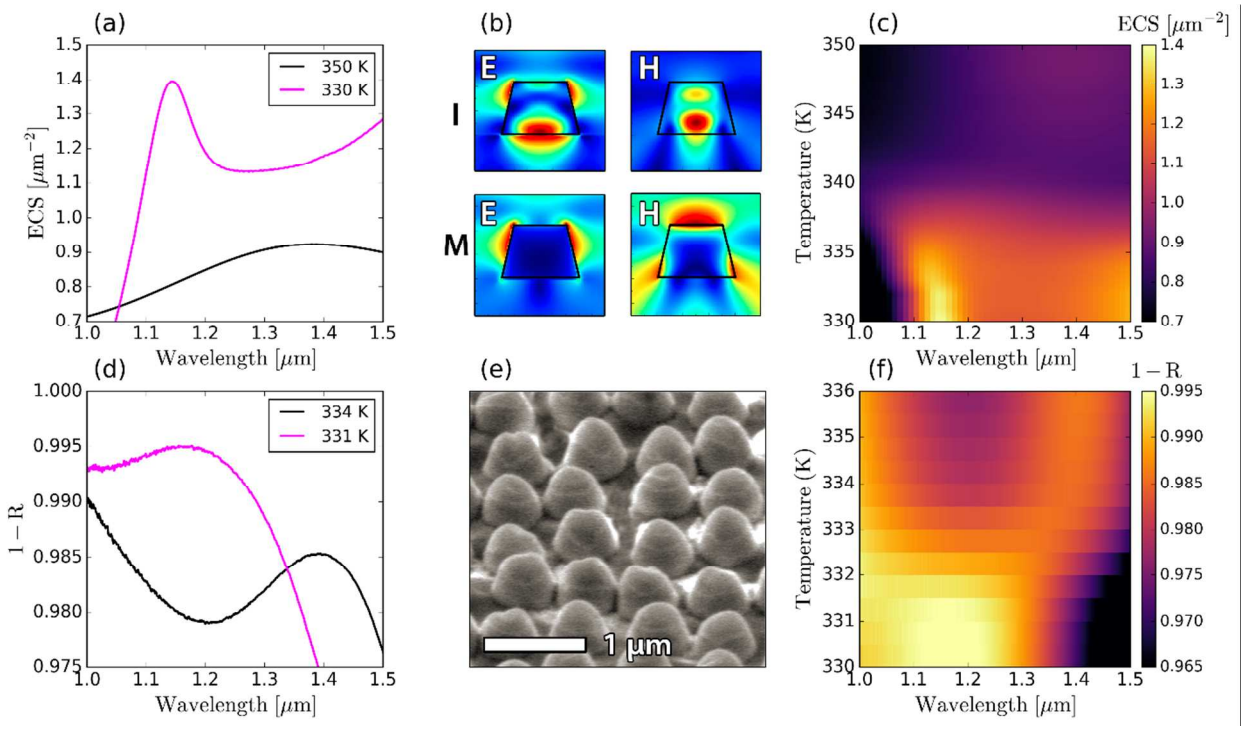

Figure S7 – **Random Arrays of VO_2 Resonators. (a)** Simulated extinction-cross-section of an individual VO_2 resonator in its insulating and metallic phases. The resonator is cone shaped with a height 500 nm, upper thickness 400 nm, and lower thickness 600 nm. **(b)** Electric and magnetic field plots of the resonators at the local maxima of the insulating and metallic phase. **(c)** Color plot of the resonator in (a), including intermediate temperatures. **(d)** Experimentally-measured FTIR reflectivity of a random array of VO_2 disk resonators in their insulating and metallic phases. **(e)** SEM of the random VO_2 arrays on a sapphire substrate. **(f)** Color plot of the experimental data in (e), including intermediate temperatures.

In Fig. S7d we plot the experimentally determined scattering response of a randomly array of VO_2 resonators. Due to random variations in spacing (SEM shown in Fig. S7e) inter-particle interference is averaged out, and the collective response of 1-R approximately corresponds to the scattering cross section, although with small shifts in resonance position and more pronounced changes in the overall amplitude. In the insulating phase (magenta) we see a peak at λ=1.2 µm. As the VO_2 is heated this peak broadens, slightly blue-shifts, and then red-shifts into a plasmonic resonance at λ=1.4 µm.

TM Polarized Wire Arrays

We now consider the case of transverse-magnetic (TM) polarized illumination, in which the electric-field is polarized parallel to the wire orientation. In Fig. S8a we plot the simulated reflection spectra. For the insulating phase, the spectra have a similar appearance, but with a red-shifted magnetic-dipole-like mode. In the metallic phase, the wire arrays do not support a resonance within this spectral range, and act more like an effective medium with averaged optical constants. The experimentally observed behavior in Fig. S8b contains similar features. In the insulating phase, the resonant peak is slightly blue-shifted, similar to the case of TE-polarized illumination in Fig. 3. In the simulated reflection color plot in Fig. S8c, we again see intermediate behavior in which the overall reflection is suppressed across the spectrum. This behavior is also observed experimentally in Fig. S8d.

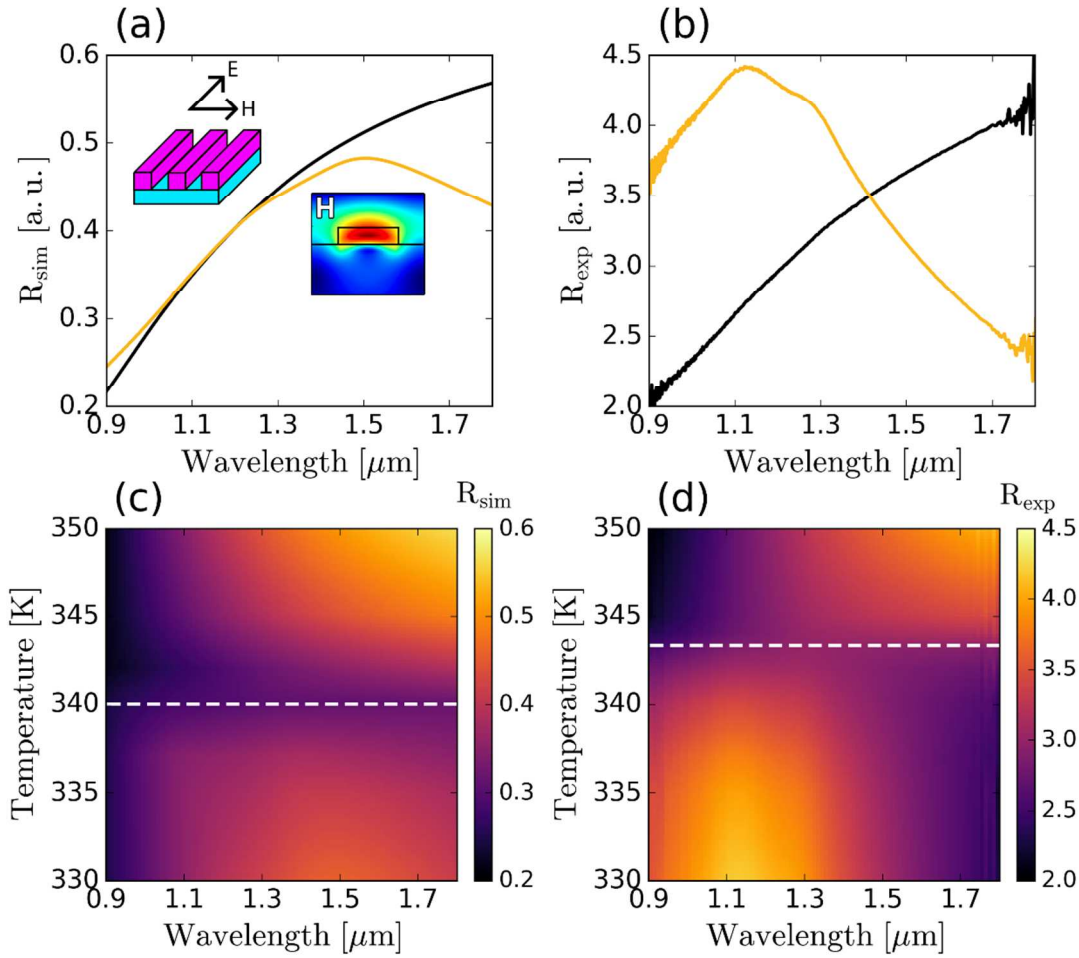

Figure S8 – **TM-Polarized VO_2 Wire Array Reflectivity. (a)** Simulated reflectivity of a VO_2 wire array, on sapphire, in the insulating and metallic phases, under TM-polarized illumination. Insets corresponding to the magnetic (electric) field profiles at the insulating (metallic) resonant peaks. **(b)** Experimentally measured reflectivity of the corresponding VO_2 wire array, in the insulating and metallic phases. **(c)** Simulated, and **(d)** experimentally measured, reflectivity of the array, including intermediate temperatures.

VO_2 Spheres

To experimentally understand the behavior of VO_2 spheres, we attempted to fabricate individual VO_2 spherical resonators using femtosecond laser ablation[7]. A femtosecond pulse was applied to a 100 nm VO_2 film which resulted in the formation of a sparse distribution of varying-size spheres. In Fig. S9a we plot the simulated scattering-cross-section of a 2 µm diameter VO_2 sphere, on a 100 nm VO_2 thin-film, on sapphire. In Fig. S9b we plot the corresponding experimentally measured reflection. In order to most accurately measure the scattering response of the VO_x sphere, rather than the evolving reflection of the thin-film, the background spectrum consisted of the area adjacent to the sphere, at the same temperature. We plot the inverted reflection spectra (1-R) to conveniently compare the experimental and calculated spectra. As can be seen from the simulation, the location of the resonant peaks between the insulator and metallic phases is almost identical for the first two resonances, even though the resonances can be assigned to fundamentally different modes. In experiments, we observe good agreement with the wavelength of the calculated peaks. Due to the relatively minor shifts however, we cannot definitively prove that this fabrication process generates VO_2 spheres with perfect stoichiometry. We performed dispersive x-ray spectroscopy (EDS) to investigate the elemental composition of the spheres. We found that there was no significant difference between the elemental analysis of the spheres and the thin-films. Due to the noise contribution by the sapphire substrate however, and the EDS system's inability to reliably determine the percentage

of light atoms such as oxygen however, we were not able to directly measure the composition of the spheres and thin-films. Further work, such as the fabrication of VO_2 spheres on non-VO_2 substrates, and more complex analysis techniques, are necessary to directly confirm the composition of the fabricated spheres.

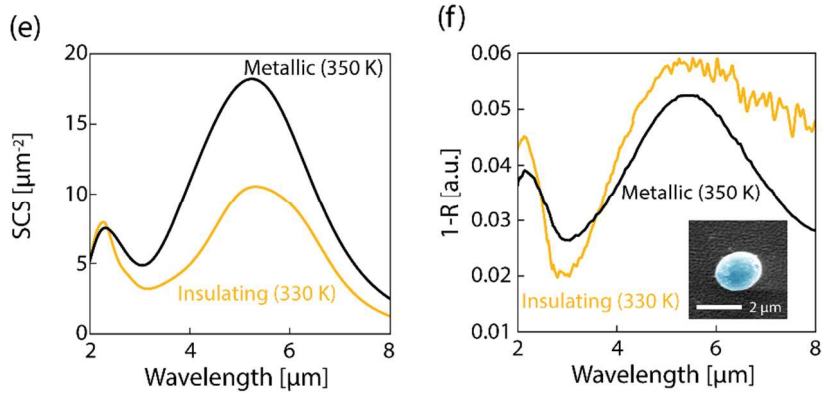

Figure S9 – **VO_2 Spheres (a)** Simulated scattering-cross-section, and **(b)** experimentally measured reflection (1-R) of a VO_2 sphere with diameter d=2 μm, on a 100 nm VO_2 thin-film, on a sapphire substrate. Inset corresponds to a false-colored SEM of the VO_2 sphere.

In Figure S10 we plot the experimentally-measured near-infrared spectra of a VO_x sphere with diameter d=2 μm in the low-temperature insulating phase (orange) and high-temperature metallic phase (black). There is a pronounced resonance shift from λ≈1.37 μm to λ≈1.43 μm across the transition. At shorter wavelengths, a peak appears in the metallic phase spectrum at λ≈1.05 μm which was not present at low temperatures. In the insulating phase, 1-R < 0 at short wavelengths, meaning that the VO_x sphere is reflecting more light than the adjacent thin-film.

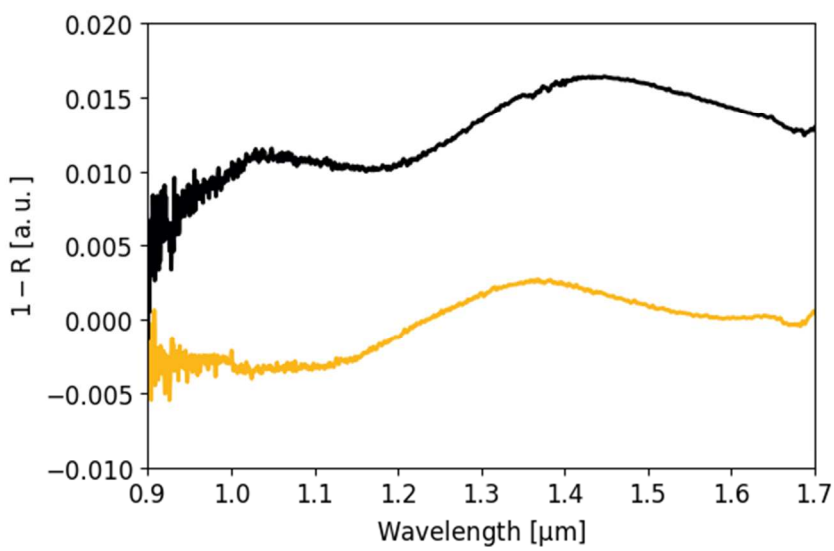

Figure S10 – **Near-Infrared Spectra of a VO_2 Sphere.** The experimentally-measured near-infrared reflection spectra of a VO_2 sphere, on a 100 nm VO_2 thin film, with diameter d = 2 μm, at 300 K (orange curve) and 360 K (black curve).

Disk Array Hysteresis Loops

In Figure S11 we plot the experimentally-measured reflection of a VO2 disk array (with approximate height 400 nm, diameter 480 nm, and pitch 500 nm) upon heating and cooling. As the disk array is heated, the resonance amplitude initially increases and then red-shifts. Upon cooling the resonance position shifts, without the increase in amplitude.

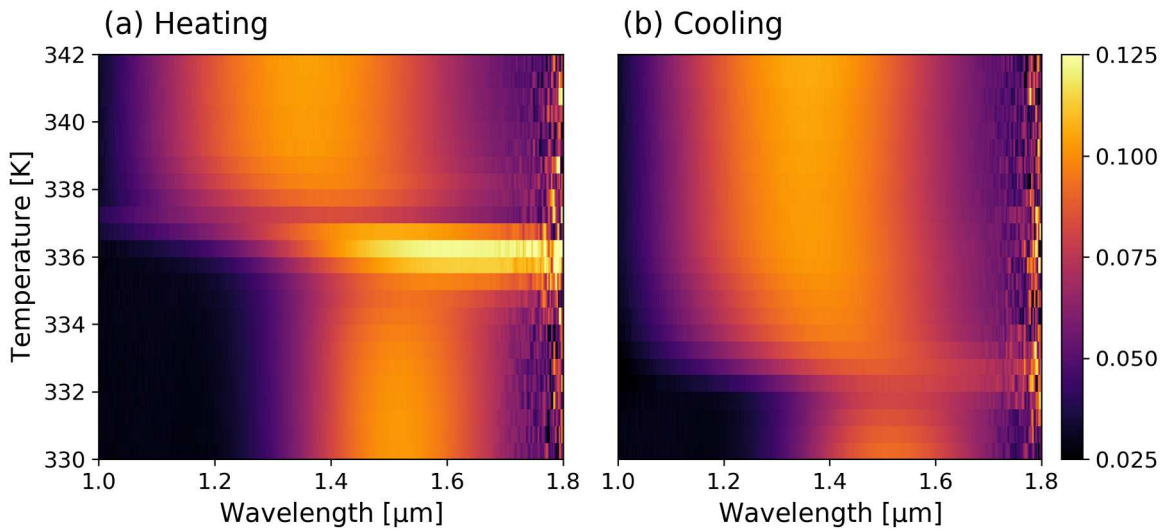

Figure S11 – Experimentally-measured reflection of a VO_2 disk array upon (a) heating, and (b) cooling. The pitch is 500 nm, the thickness is approximately 400 nm, and the diameter is approximately 480 nm.

In Figure S12 we plot the experimentally-measured reflection of a VO2 disk array with an increased diameter and pitch (approximate height 400 nm, diameter 580 nm, and pitch 600 nm) upon heating and cooling. Similar to the previous disk array, upon heating, the resonance amplitude initially increases and then red-shifts. Upon cooling the resonance position shifts, without the increase in amplitude.

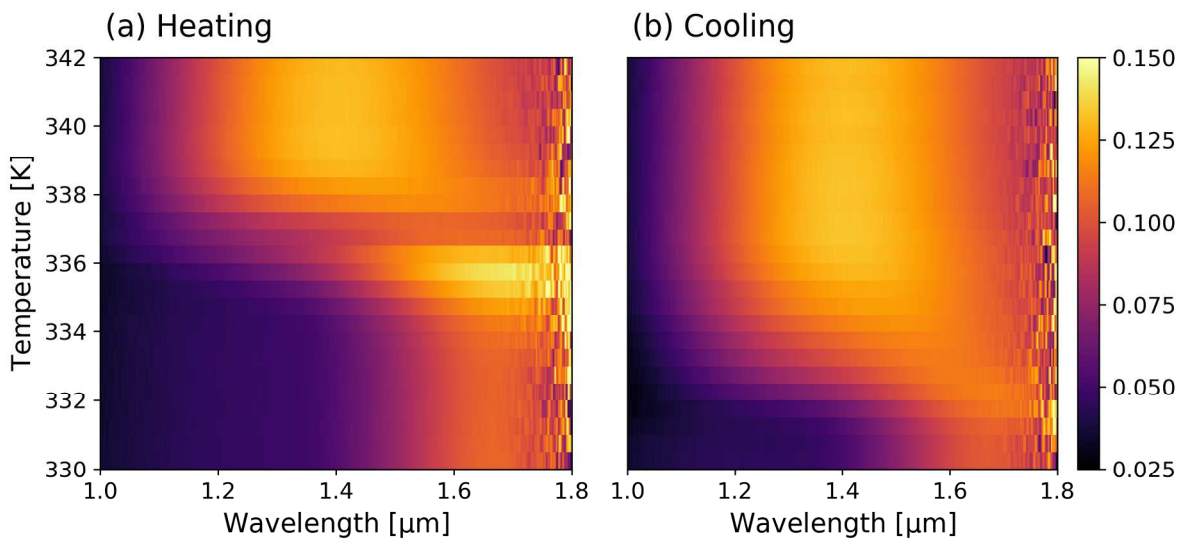

Figure S12 – Experimentally-measured reflection of a VO_2 disk array upon (a) heating, and (b) cooling. The pitch is 600 nm, the thickness is approximately 400 nm, and the diameter is approximately 580 nm.

References

1 Aramaki, S. & Roy, R. Single-crystal growth of VO2 by isothermal flux-evaporation. Journal of Materials Science, 1968, 3, 643-645.

2 Ramirez, J. G. et al. Effect of disorder on the metal-insulator transition of vanadium oxides: Local versus global effects. Phys. Rev. B, 2015, 91, 205123.

3 Pennycook, S. et al. Misfit accommodation in oxide thin film heterostructures. Acta Mater., 2013, 61, 2725-2733.

4 Valmianski, I., Ramirez, J.G., Urban, C., Batlle, X., Schuller, I.K. Deviation from bulk in the pressure-temperature phase diagram of V2O3 thin films. Phys. Rev. B, 2017, 95, 155132.

5 Hightower, R. L., & Richardson, C. B. (1988). Resonant Mie scattering from a layered sphere. Applied optics, 27(23), 4850-4855.

6 Bohren, C. F. & Huffman, D. R. Absorption and scattering of light by small particles. John Wiley & Sons, 2008.

7 Evlyukhin, A. B. et al. Demonstration of magnetic dipole resonances of dielectric nanospheres in the visible region. Nano Lett., 2012, 12, 3749-3755.